Int J Thermophys (2009) 30:1055–1073
DOI 10.1007/s10765-009-0605-3

Multiple Scattering of Thermal Waves from a Subsurface Cylindrical Inclusion in Semi-infinite Functionally Graded Materials Using Non-Fourier Model

Xue-Qian Fang · Shu-Min Duan · Shu-Hong Liu · Xiao-Hua Wang · Wen-Jie Feng

Received: 20 October 2008 / Accepted: 29 May 2009 / Published online: 16 June 2009

Abstract In this study, a theoretical method is applied to investigate the multiple scattering of thermal waves and temperature field resulting from a subsurface cylindrical inclusion in a semi-infinite functionally graded material (FGM). The adiabatic boundary condition at the semi-infinite surface is considered. The thermal waves are excited at the surface of semi-infinite functionally graded materials by modulated optical beams. The model includes the multiple scattering effects of the cylindrical thermal wave generated by the line heat source. According to the wave equation of heat conduction, a general solution of scattered thermal waves is presented. Numerical calculations illustrate the effect of subsurface inclusion on the temperature and phase change at the sample surface under different physical and geometrical parameters. It is found that the temperature above the conducting cylindrical inclusion decreases because of the existence of the inclusion. The effect of the inclusion on the temperature and phase change at the surface is also related to the non-homogeneous parameter of FGMs, the wave frequency of thermal waves, and the distance between the inclusion and the semi-infinite surface. Finally, the effect of the relaxation time of buried inclusion on the temperature and phase change at the surface is examined.

Keywords Cylindrical inclusion · Multiple scattering of thermal waves · Non-Fourier heat conduction law · Semi-infinite functionally graded materials

X.-Q. Fang (✉) · S.-M. Duan · S.-H. Liu · W.-J. Feng
Department of Engineering Mechanics, Shijiazhuang Railway Institute, Shijiazhuang 050043, China
e-mail: fangxueqian@163.com

X.-H. Wang
Computer and Information Engineering Department, Shijiazhuang Railway Institute, Shijiazhuang 050043, China

List of Symbols

λ	Thermal conductivity of FGMs
c_p	Specific heat capacity of FGMs
ρ	Mass density of FGMs
D	Thermal diffusivity of FGMs
τ	Relaxation time of FGMs
λ_1	Thermal conductivity of the inclusion
c_{p1}	Specific heat capacity of the inclusion
ρ_1	Mass density of the inclusion
D_1	Thermal diffusivity of the inclusion
τ_1	Relaxation time of the inclusion
a	Radius of fibers
b	Buried depth of the subsurface cylindrical inclusion
f	Frequency of ultrashort laser pulse
σ	Spatial variational exponent of physical parameters
∇	Hamiltonian operator
T	Temperature in composite materials
c	Propagation speed of thermal waves in FGMs
c_1	Propagation speed of thermal waves in the inclusion
T_0	Average temperature
ω	Incident frequency of thermal waves
ϑ	Wave field of thermal waves
κ	Propagating wave number of complex variables
k	Wave number of thermal waves without diffusive effect
α	Wave number of thermal waves
β	Absorption coefficient of thermal waves
ϑ_0	Temperature amplitude of incident thermal waves
$J_n(\cdot)$	nth Bessel function of the first kind
$H_n(\cdot)$	nth Hankel function of the first kind
A_n^l, B_n^l, C_n^l, E_n^l	Mode coefficients

Subscripts

1 Actual inclusion
2 Image inclusion
l Reflected time

Superscripts

(in) Incident thermal wave
(s) Scattered thermal wave
(r) Refracted thermal wave in the inclusion
(t) Total temperature field in FGMs

1 Introduction

The thermal wave method is an efficient tool for the nondestructive evaluation (NDE) of opaque materials. Thermal waves are generated in a material as a consequence of the absorption of an intensity modulated light beam. These highly damped thermal waves propagate through the material and are scattered by the buried heterogeneities. Different photothermal methods can be used to detect the subsequent modulated temperature field at the sample surface: "mirage" effect technique, infrared (IR) radiometry, thermo-reflectance, etc. Their selection depends mainly on the optical and thermal properties of the sample. The main goal of this methodology is to retrieve the geometrical (size, depth, orientation), and if possible, the thermal characteristics of the subsurface scattering features. Due to its noncontact, nondestructive, and highly sensitive nature, photothermal radiometry (PTR) has recently become a powerful tool for the thermal characterization and nondestructive evaluation of broad classes of materials.

First, Ocariz et al. applied photothermal method to locate and characterize the geometrical and thermal properties of the buried cylinder theoretically [1] and experimentally [2]. Subsequently, Salazar et al. [3] used this method to calculate the in-plane effective thermal diffusivity of unidirectional fiber-reinforced composites. Salazar and co-workers also extended this classical flash method to study the surface temperature resulting from nonplanar samples, such as solid cylinders [4], hollow cylinders [5,6], and spheres [7]. Recently, Madariaga and Salazar [8] exploited this elegant method to express the surface temperature of multilayered spherical samples with continuously varying in-depth thermal conductivity. In a series of studies of Wang et al. [9], photothermal radiometry (PTR) was used for the quantitative nondestructive evaluation of samples with curved surfaces, cylindrical composite structures [10], and spherical geometries [11].

Functionally graded materials (FGMs) are the new generation of composites, and is an important area of materials science research. The volume fraction of materials changes gradually, and the non-homogeneous microstructures in the materials produce continuously graded macroscopic properties, such as the heat conductivity, specific heat, and mass density. All the properties have many potential applications, e.g., thermal barrier coatings, thermal protection of reentry capsules, furnace liners, personal body armor, and materials of elevated temperature and heat resistance for electromagnetic sensors [12]. In an ideal FGM, the material properties may vary smoothly along one direction. As an example, having a smooth transition region between a pure metal and pure ceramic would result in a new type of material, which combines the desirable high-temperature properties and thermal resistance of a ceramic with the fracture toughness of a metal. With the wide application of FGMs in engineering, it is desirable to apply nondestructive evaluation (NDE) to retrieve the geometrical (size, depth, orientation) and thermal characteristics of the subsurface scattering features in FGMs.

Different physical parameters and boundary conditions of subsurface defects have great effects on the propagation and diffusion of thermal waves, which are directly represented by the temperature field at the surface of FGMs. By using the detecting system of thermal waves and measuring the changes of temperature at the surface of FGMs,

the properties of internal structures can be obtained for purposes of detection and inspection [13]. The non-destructive detection technology is of considerable importance in the research of designing new FGMs in aerospace engineering, and improving the reliability of industrial products and facilities.

At present, in infrared thermal imaging, the physical models applied to determine the temperature distribution of the sample with defects are still based on the classical Fourier heat conduction law. Namely, parabolic equation of heat diffusion is often applied to compute and analyze this model [14,15]. The classical Fourier law is quite accurate for the heat conduction in most common engineering situations. However, for situations involving very short times or extreme thermal gradients resulting from the graded properties of materials, Fourier's law becomes invalid. So, the non-Fourier heat conduction law was developed. The wave models, which can describe the relaxation behavior of heat conduction, represent the modifications for the classical theory of Fourier heat conduction. When the equations of heat conduction and energy are incorporated, the hyperbolic equation of heat conduction can be obtained. In many cases (e.g., laser heating, multilayer insulation at the low temperature, superconducting film, etc.), non-Fourier heat conduction is encountered [16,17]. Recently, Ma and Tan [18] have applied the non-Fourier heat conduction model and wave function expansion method to analyze the temperature distribution at the surface of functionally graded materials resulting from subsurface spheroids.

To the authors' knowledge, photothermal methods have not been applied to study the semi-infinite functionally graded material with a cylindrical inclusion. The main objective of this study is to investigate the multiple scattering of thermal waves resulting from an embedded cylindrical inclusion in a semi-infinite functionally graded material, and the adiabatic boundary condition at the surface is considered. The non-Fourier heat conduction law is applied to deal with the graded properties of FGMs, and the hyperbolic equation of heat conduction is solved by employing the wave function expansion method. The expanded mode coefficients are determined by satisfying the boundary conditions of cylindrical inclusion and semi-infinite surface. The adiabatic boundary condition at the semi-infinite surface is satisfied by using the image method. The analytical solution of the temperature field at the surface of FGMs is presented. The effects of incident wave number and the structural and physical parameters of FGMs on the temperature distribution at the semi-infinite surface are analyzed.

2 Thermodynamic Equation of Thermal Wave Propagation and Its Solution

A semi-infinite functionally graded material is considered, as depicted in Fig. 1. A cylindrical inclusion of radius a is embedded in the FGM structure. The depth of the center of cylindrical inclusion beneath the surface is b. The thermal conductivity, thermal diffusivity, specific heat at constant pressure, and density of the cylindrical inclusion are denoted as λ_1, D_1, c_{p1}, and ρ_1. Let an ultrashort laser pulse modulated at frequency f hit the surface of heated materials along the x direction. The thermal waves are generated in FGMs. Based on the non-Fourier law of heat conduction, the governing equation of temperature in the materials, as utilized in a previous investigation [19], can be written as

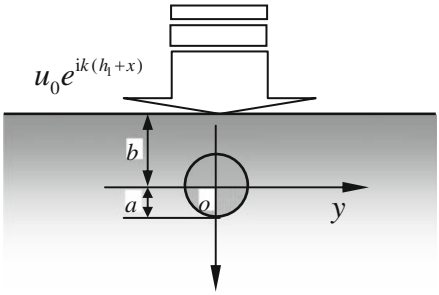

Fig. 1 Schematic of the embedded inclusion and the incident thermal waves in a semi-infinite functionally graded material

$$\nabla \cdot (\lambda \nabla T) = \rho c_p \left(\frac{\partial T}{\partial t} + \tau \frac{\partial^2 T}{\partial t^2} \right). \tag{1}$$

where $\nabla = \mathrm{i}\partial/\partial x + \mathrm{j}\partial/\partial y$ is the Hamiltonian operator and λ, c_p, and ρ are the thermal conductivity, the specific heat at constant pressure, and the density of FGMs, respectively; τ is the exponential relaxation time needed for reaching new equilibrium in FGMs, and T is the temperature in FGMs. It should be noted that the exponential relaxation time is a thermodynamic property of the materials.

Assume that the density and relaxation time of materials are constants. The thermal conductivity and the specific heat at constant pressure of FGMs vary gradually along the x direction. The variations of them have an exponential form [20–22], namely,

$$\lambda = \lambda_0 \exp(2\sigma x), \quad c_p = c_{p0} \exp(2\sigma x). \tag{2}$$

Here λ_0 and c_{p0} denote the thermal conductivity and the specific heat at the position of $x = 0$, respectively. σ is the spatial variational exponent of physical parameters, and denotes the non-homogeneous property of FGMs.

Substituting Eq. 2 into Eq. 1, the following equation can be obtained:

$$\nabla^2 T + 2\sigma \frac{\partial T}{\partial x} = \frac{1}{c^2} \frac{\partial^2 T}{\partial t^2} + \frac{1}{D} \frac{\partial T}{\partial t}, \tag{3}$$

where D ($D = \lambda/\rho c_p = \lambda_0/\rho c_{p0}$) is the thermal diffusivity of FGMs and $c = \sqrt{D/\tau}$ is the propagation speed of thermal waves.

The solution of a periodic steady state is investigated. Assuming that $T = T_0 + Re[\vartheta \exp(-\mathrm{i}\omega t)]$, the following equation can be derived in terms of Eq. 3:

$$\nabla^2 \vartheta + 2\sigma \frac{\partial \vartheta}{\partial x} + \left(\frac{\omega^2}{c^2} + \frac{\mathrm{i}\omega}{D} \right) \vartheta = 0, \tag{4}$$

where T_0 is the average temperature, $\omega = 2\pi f$ is the incident frequency, and $\mathrm{i} = \sqrt{-1}$ is the imaginary unit.

Thus, the solution of Eq. 4 takes the following form:

$$\vartheta = \exp(-\sigma x) u(x, y), \tag{5}$$

in which the function $u(x, y)$ should satisfy the following equation:

$$\nabla^2 u + \kappa^2 u = 0, \tag{6}$$

where $\kappa = \left(\frac{\omega^2}{c^2} + \frac{\mathrm{i}\omega}{D} - \sigma^2\right)^{1/2} = \alpha + \mathrm{i}\beta$ is the wave number of complex variables, and α, β are the wave number and the absorption coefficient of thermal waves, respectively. Without loss of generality, after normalizing and taking $\alpha > 0$, $\beta > 0$, one can obtain

$$\begin{aligned}\alpha &= \sqrt{\frac{1}{2}\left[\sqrt{\left(\frac{\omega^2}{c^2} - (\sigma^2)\right)^2 + \left(\frac{\omega}{D}\right)^2} + \frac{\omega^2}{c^2} - \sigma^2\right]} \\ &= \sqrt{\frac{1}{2}\left[\sqrt{(k^2 - \sigma^2)^2 + \frac{4}{\mu^4}} + k^2 - \sigma^2\right]}. \end{aligned} \tag{7}$$

$$\begin{aligned}\beta &= \sqrt{\frac{1}{2}\left[\sqrt{\left(\frac{\omega^2}{c^2} - \sigma^2\right)^2 + \left(\frac{\omega}{D}\right)^2} - \frac{\omega^2}{c^2} + \sigma^2\right]} \\ &= \sqrt{\frac{1}{2}\left[\sqrt{(k^2 - \sigma^2)^2 + \frac{4}{\mu^4}} + k^2 + \sigma^2\right]}. \end{aligned} \tag{8}$$

Here k is the wave number of thermal waves without the diffusive effect. When the propagating speed of thermal waves is $c \to \infty$ and the non-homogeneous parameter is $\sigma \to 0$, one can obtain $\alpha \to \sqrt{\frac{\omega}{2D}} = \frac{1}{\mu}$ and $\beta \to \sqrt{\frac{1}{2}\frac{\omega}{D}} = \frac{1}{\mu}$. So, the wave number of thermal waves is $\kappa = \alpha + \mathrm{i}\beta \quad \to (1 + \mathrm{i})\frac{1}{\mu}$. In this way, the hyperbolic equation of heat conduction in the graded materials can be reduced to the classical equation of Fourier heat conduction.

According to Eqs. 4, 5, and 6, one can see that in FGMs there exists the wave motion with the form of $\vartheta \mathrm{e}^{-\mathrm{i}\omega t} = \vartheta_0 \exp(-\sigma x)\mathrm{e}^{\mathrm{i}(\alpha x - \omega t)}$. The wave modes denote the propagating thermal waves with its amplitude of vibration attenuating in the x direction.

The general solution of the scattered field of thermal waves in graded materials determined by Eq. 5 can be described as

$$\vartheta^{(\mathrm{s})} = \mathrm{e}^{-\sigma x} \sum_{n=-\infty}^{\infty} A_n H_n(\kappa r)\mathrm{e}^{\mathrm{i}n\theta}, \tag{9}$$

where $H_n(\cdot)$ is the Hankel function of the first kind, A_n are the mode coefficients resulting from the subsurface cylindrical inclusion, and the superscript (s) stands for the scattered waves. Note that the mode coefficients are determined by satisfying the boundary conditions of inclusions.

3 Incidence of Thermal Waves and Total Wave Field

Thermal waves can be generated at the surface of graded materials by the laser beam with a modulated ultrashort pulse. Assume that a periodic steady thermal wave propagates along the positive x direction. According to the wave function expansion method [4], the incident waves can be described as

$$\vartheta_1^{(\mathrm{in})} = \vartheta_0 \exp(\mathrm{i}\kappa b)\mathrm{e}^{\mathrm{i}\kappa x} = \vartheta_0 \exp(\mathrm{i}\kappa b) \sum_{n=-\infty}^{\infty} \mathrm{i}^n J_n(\kappa r)\mathrm{e}^{\mathrm{i}n\theta}, \tag{10}$$

where w_0 is the temperature amplitude of incident thermal waves, κ is the wave number of incident waves, and the superscript (in)denotes the incident thermal wave.

When the thermal wave propagates in the semi-infinite structure, it is scattered by the cylindrical inclusion at first. Then, the outgoing scattered waves are reflected by the semi-infinite surface. The reflected waves $\vartheta^{(\mathrm{f})}$are scattered by the cylindrical inclusion again. This complex phenomenon is shown in Fig. 1.

To satisfy the adiabatic boundary conditions at the semi-infinite surface, the image method is applied, as shown in Fig. 2. The reflected waves at the semi-infinite surface are described by the virtual image inclusions.

For the image cylindrical inclusion, the thermal waves propagate in the negative x' direction, and are described as

$$\vartheta_2^{(\mathrm{in})} = \vartheta_0 \exp(\mathrm{i}\kappa b)\mathrm{e}^{-\mathrm{i}\kappa x'} = \vartheta_0 \exp(\mathrm{i}\kappa b) \sum_{n=-\infty}^{\infty} \mathrm{i}^{-n} J_n(\kappa r')\mathrm{e}^{\mathrm{i}n\theta'}. \tag{11}$$

In the local coordinate system (r, θ) of the real inclusion, the scattered field of thermal waves resulting from the subsurface inclusion can be described as

$$\vartheta_1^{(\mathrm{s})} = \exp(-\sigma x) \sum_{l=1}^{\infty} \sum_{n=-\infty}^{\infty} A_n^l H_n(\kappa r)\mathrm{e}^{\mathrm{i}n\theta}. \tag{12}$$

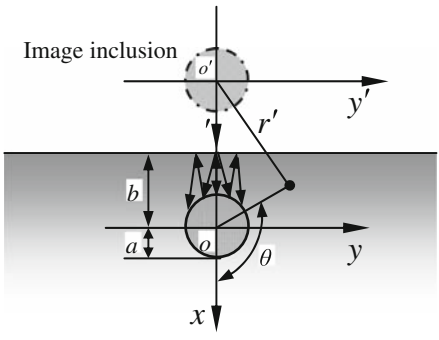

Fig. 2 Schematic of image method in a semi-infinite functionally graded material

In the local coordinate (r', θ') of the image inclusion, the scattered field resulting from the image inclusion can be described as

$$\vartheta_2^{(\mathrm{s})} = \exp(\sigma x') \sum_{l=1}^{\infty} \sum_{n=-\infty}^{\infty} B_n^l H_n(\kappa r') \mathrm{e}^{\mathrm{i}n\theta'}, \tag{13}$$

It should be noted that A_n^l and $B_n^l (l = 1, 2, \ldots, \infty)$ are the lth thermal wave mode coefficients of the real and image inclusions, respectively. They can be determined by satisfying the boundary condition of the subsurface inclusion.

Thus, the total wave field near the actual and image inclusions in graded materials is taken to be the superposition of the incident waves, the scattered waves and the reflected waves at the surface, i.e.,

$$\vartheta_1^{(\mathrm{t})} = \vartheta_1^{(\mathrm{in})} + \vartheta_1^{(\mathrm{s})} + \vartheta_1^{(\mathrm{f})} = \vartheta_1^{(\mathrm{in})} + \vartheta_1^{(\mathrm{s})} + \vartheta_2^{(\mathrm{s})}. \tag{14}$$

$$\vartheta_2^{(\mathrm{t})} = \vartheta_2^{(\mathrm{in})} + \vartheta_2^{(\mathrm{s})} + \vartheta_2^{(\mathrm{f})} = \vartheta_2^{(\mathrm{in})} + \vartheta_2^{(\mathrm{s})} + \vartheta_1^{(\mathrm{s})}. \tag{15}$$

Similarly, part of the incident wave is refracted into the cylindrical inclusions. Inside the actual and image cylindrical inclusions, the refracted wave is a standing wave and it is expanded as

$$\vartheta_1^{(\mathrm{r})} = \sum_{l=1}^{\infty} \sum_{n=-\infty}^{\infty} C_n^l J_n(\kappa_c r) \mathrm{e}^{\mathrm{i}n\theta}. \tag{16}$$

$$\vartheta_2^{(\mathrm{r})} = \sum_{l=1}^{\infty} \sum_{n=-\infty}^{\infty} E_n^l J_n(\kappa_c r') \mathrm{e}^{\mathrm{i}n\theta'}. \tag{17}$$

where C_n^l and E_n^l are the lth mode coefficients of the refracted waves, and $\kappa_{\mathrm{c}} = \left(\frac{\omega^2}{c_1} + \frac{\mathrm{i}\omega}{D_1}\right)^{1/2}$ with

$$c_1 = \sqrt{D_1/\tau_1}, \tag{18}$$

where τ_1 is the relaxation time of the cylindrical inclusion.

To make the computation tractable, the expression of temperature fields in the local coordinate system (r', θ') should be translated into another local coordinate system (r, θ). According to the addition theorem for Hankel functions [23], the following relation can be derived:

$$H_n(\kappa r') \mathrm{e}^{\mathrm{i}n\theta'} = \sum_{m=-\infty}^{\infty} (-1)^{m-n} H_{m-n}(2\kappa b) J_m(\kappa r) \mathrm{e}^{\mathrm{i}m\theta}. \tag{19}$$

Similarly,

$$H_n(\kappa r)\mathrm{e}^{\mathrm{i}n\theta} = \sum_{m=-\infty}^{\infty} H_{m-n}(2\kappa b)J_m(\kappa r')\mathrm{e}^{\mathrm{i}m\theta'}. \tag{20}$$

So, the following translation of coordinate systems can be obtained:

$$\exp(\sigma r'\cos\theta')\sum_{n=-\infty}^{\infty} H_n(\kappa r')\mathrm{e}^{\mathrm{i}n\theta'} = \exp[\sigma(2b + r\cos\theta)] \times \sum_{n=-\infty}^{\infty}\sum_{m=-\infty}^{\infty}(-1)^{m-n}H_{m-n}(2\kappa b)J_m(\kappa r)\mathrm{e}^{\mathrm{i}m\theta}, \tag{21}$$

where $r' = \sqrt{r^2 + 4b^2 + 4rb\cos\theta}$, and $\cos\theta' = \dfrac{(r')^2 + 4b^2 - r^2}{4br'}$.

$$\exp(-\sigma r\cos\theta)\sum_{n=-\infty}^{\infty} H_n(\kappa r)\mathrm{e}^{\mathrm{i}n\theta} = \exp[\sigma(2b - r'\cos\theta')]\sum_{n=-\infty}^{\infty}\sum_{m=-\infty}^{\infty} H_{m-n}(2\kappa b)J_m(\kappa r')\mathrm{e}^{\mathrm{i}m\theta'}, \tag{22}$$

where $r = \sqrt{(r')^2 + 4b^2 - 4r'b\cos\theta'}$, and $\cos\theta = -\dfrac{r^2 + 4b^2 - (r')^2}{4br}$.

4 Boundary Conditions Around the Cylindrical Inclusion

In this study, a conducting cylindrical inclusion is considered. The boundary conditions around the inclusion are expressed as

$$\vartheta^{(t)} = \vartheta^{(r)}, \quad q_{\mathrm{r}}^{(t)} = q_{\mathrm{r}}^{(r)} \quad \text{for} \quad r = a, \tag{23}$$

where q_{r} is the heat flow density in the radial direction corresponding to ϑ, and $q_{\mathrm{r}} = -\lambda\frac{\partial\vartheta}{\partial r}$.

5 Mode Coefficient of Waves and Distribution of Temperature

Multiple scattering of thermal waves takes place between the actual and image inclusions. By satisfying the boundary conditions around the inclusions, the mode coefficients of thermal waves are determined. Substituting Eqs. 15–18 into Eq. 23, multiplying both sides of Eq. 23 by $\mathrm{e}^{-\mathrm{i}s\theta}$, and then integrating from $-\pi$ to π, the following recurrence formula can be obtained:

when $l = 1$, the relations among every mode coefficient of the scattered waves are written as

$$A_{\mathrm{s}}^{1} \exp(-\sigma a \cos\theta) H_{\mathrm{s}}(\kappa a) - C_{\mathrm{s}}^{1} J_{\mathrm{s}}(\kappa_{\mathrm{c}} a) = -\mathrm{i}^{\mathrm{s}} \exp(\mathrm{i}\kappa b) J_{\mathrm{s}}(\kappa a), \tag{24}$$

$$A_{s}^{1} \exp(-\sigma a \cos\theta) \{-\sigma a \cos\theta H_{\mathrm{s}}(\kappa a) + [s H_{\mathrm{s}}(\kappa a) - \kappa a H_{\mathrm{s}+1}(\kappa a)]\} - \frac{\lambda_1}{\lambda} C_{\mathrm{s}}^{1} \times \left[s J_{\mathrm{s}}(\kappa_{\mathrm{c}} a) - \kappa_{\mathrm{c}} a J_{\mathrm{s}+1}(\kappa_{\mathrm{c}} a)\right] = -\mathrm{i}^{\mathrm{s}} \exp(\mathrm{i}\kappa b) \left[s J_{\mathrm{s}}(\kappa a) - \kappa a J_{\mathrm{S}+1}(\kappa a)\right], \tag{25}$$

$$B_{\mathrm{s}}^{1} \exp(\sigma a \cos\theta') H_{\mathrm{s}}^{(1)}(\kappa a) - E_{\mathrm{s}}^{1} J_{\mathrm{s}}(\kappa_{\mathrm{c}} a) = -\mathrm{i}^{-\mathrm{s}} \exp(\mathrm{i}\kappa b) J_{\mathrm{s}}(\kappa a), \tag{26}$$

$$B_{\mathrm{s}}^{1} \exp(\sigma a \cos\theta') \{\sigma a \cos\theta' H_{\mathrm{s}}(\kappa a) + [s H_{\mathrm{s}}(\kappa a) - \kappa a H_{\mathrm{S}+1}(\kappa a)]\} - \frac{\lambda_1}{\lambda} E_{\mathrm{s}}^{1} \times \left[s J_{\mathrm{s}}(\kappa_{\mathrm{c}} a) - \kappa_{\mathrm{c}} a J_{\mathrm{s}+1}(\kappa_{c} a)\right] = -\mathrm{i}^{-\mathrm{S}} \exp(\mathrm{i}\kappa b)[s J_{\mathrm{s}}(\kappa a) - \kappa a J_{\mathrm{s}+1}(\kappa a)], \tag{27}$$

when $l = 2, 3, \ldots, \infty$, the relations among every mode coefficient of the thermal waves are written as

$$\begin{aligned} &\exp(-\sigma a \cos\theta) H_{\mathrm{s}}^{(1)}(\kappa a) A_{\mathrm{s}}^{l} - C_{\mathrm{s}}^{l} J_{\mathrm{s}}(\kappa_{\mathrm{c}} a) \\ &\quad = -B_{\mathrm{s}}^{l-1} \exp[\sigma(2b + a\cos\theta)] \\ &\qquad \times \sum_{n=-\infty}^{\infty} (-1)^{\mathrm{s}-n} H_{\mathrm{s}-n}(2\kappa b) J_{\mathrm{s}}(\kappa a), \quad (l = 2, 3, \ldots, \infty), \end{aligned} \tag{28}$$

$$\begin{aligned} &A_{s}^{l} \exp(-\sigma a \cos\theta)\{-\sigma a \cos\theta H_{\mathrm{s}}(\kappa a) + [s H_{\mathrm{s}}(\kappa a) - \kappa a H_{\mathrm{s}+1}(\kappa a)]\} \\ &\quad - \frac{\lambda_1}{\lambda} C_{\mathrm{s}}^{1} [s J_{\mathrm{s}}(\kappa_{\mathrm{c}} a) - \kappa_{\mathrm{c}} a J_{\mathrm{s}+1}(\kappa_{\mathrm{c}} a)] \\ &\quad = -B_{\mathrm{s}}^{l-1} \exp[\sigma(2b + a\cos\theta)] \left\{ \sigma a \cos\theta \sum_{n=-\infty}^{\infty} (-1)^{\mathrm{s}-\mathrm{n}} H_{\mathrm{s}-\mathrm{n}}(2\kappa b) J_{\mathrm{s}}(\kappa a) \right. \\ &\qquad \left. + \sum_{n=-\infty}^{\infty} (-1)^{\mathrm{s}-n} H_{\mathrm{s}-\mathrm{n}}(2\kappa b)[s J_{\mathrm{s}}(\kappa a) - \kappa a J_{\mathrm{s}+1}(\kappa a)] \right\}, \end{aligned} \tag{29}$$

$$\begin{aligned} &\exp(\sigma a \cos\theta') H_{\mathrm{s}}(\kappa a) B_{\mathrm{s}}^{l} - E_{\mathrm{s}}^{l} J_{\mathrm{s}}(\kappa_{\mathrm{c}} a) \\ &\quad = -A_{\mathrm{s}}^{l-1} \exp[\sigma(2b - a\cos\theta')] \\ &\qquad \times \sum_{n=-\infty}^{\infty} H_{\mathrm{s}-n}(2\kappa b) J_{\mathrm{s}}(\kappa a), \quad (l = 2, 3, \ldots, \infty), \end{aligned} \tag{30}$$

$$B_s^l \exp(\sigma a \cos\theta')\{\sigma a \cos\theta' H_s(\kappa a) + [sH_s(\kappa a) - \kappa a H_{s+1}(\kappa a)]\} - \frac{\lambda_1}{\lambda} E_s^1 [sJ_s(\kappa_c a) - \kappa_c a J_{s+1}(\kappa_c a)]$$
$$= -A_s^{l-1} \exp[\sigma(2b - a\cos\theta')] \left\{ -\sigma a \cos\theta' \sum_{n=-\infty}^{\infty} H_{s-n}(2\kappa b) J_s(\kappa a) + \sum_{n=-\infty}^{\infty} H_{s-n}(2\kappa b)[sJ_s(\kappa a) - \kappa a J_{s+1}(\kappa a)] \right\}, \tag{31}$$

Equations 24–31 are the infinite algebraic equations determining the mode coefficients of thermal waves.

In the following analysis, it is convenient to make the variables dimensionless. To accomplish this step, we may introduce a characteristic length, a, where a is the radius of the subsurface inclusion. The following dimensionless variables and quantities have been chosen for computation: the ratio of embedded depth is $b^* = b/a = 1.5$ to 3.0, and the non-homogeneous parameter of FGMs is $\sigma^* = \sigma a = -1.0$ to 1.0. The ratio of the thermal conductivity is $\lambda^* = \lambda_1/\lambda_0 = 2.0$ to 50.0, $\tau^* = \tau_1/\tau = 10^1$ to 10^5, and $D^* = D_1/D_0 = 2.0$ to 50.0. The dimensionless temperature is $\vartheta^* = \vartheta/\vartheta_0$. Thus, the dimensionless complex wave number is $\kappa^* = \kappa a = \alpha a + \mathrm{i}\beta a$, and they are written as

$$\alpha a = \sqrt{\sqrt{\frac{1}{4}\left[(ka)^2 - (\sigma a)^2\right]^2 + \left(\frac{a}{\mu}\right)^4} + \frac{1}{2}\left[(ka)^2 - (\sigma a)^2\right]}, \tag{32}$$

$$\beta a = \sqrt{\sqrt{\frac{1}{4}\left[(ka)^2 - (\sigma a)^2\right]^2 + \left(\frac{a}{\mu}\right)^4} - \frac{1}{2}\left[(ka)^2 + (\sigma a)^2\right]}. \tag{33}$$

So, the expression of the temperature distribution at the surface of graded materials is written as

$$\vartheta = \vartheta_0 \exp(\mathrm{i}\kappa b) \sum_{n=-\infty}^{\infty} \mathrm{i}^n J_n(\kappa r) \mathrm{e}^{\mathrm{i}n\theta} + \exp(-\sigma x) \sum_{l=1}^{\infty} \sum_{n=-\infty}^{\infty} A_n^l H_n(\kappa r) \mathrm{e}^{\mathrm{i}n\theta}$$
$$+ \exp[\sigma(2b + a\cos\theta)] \sum_{l=1}^{\infty} \sum_{n=-\infty}^{\infty} \sum_{m=-\infty}^{\infty} (-1)^{m-n} B_n^l H_{m-n}(2\kappa b) J_m(\kappa r) \mathrm{e}^{\mathrm{i}m\theta}. \tag{34}$$

here $x = 0$ to 2.

6 Numerical Examples

If there exists a defect in the materials, the multiple scattering of thermal waves between the subsurface cylinder and the surface will occur, which influences the distribution of temperature at the surface of graded materials. Periodic heating will bring about

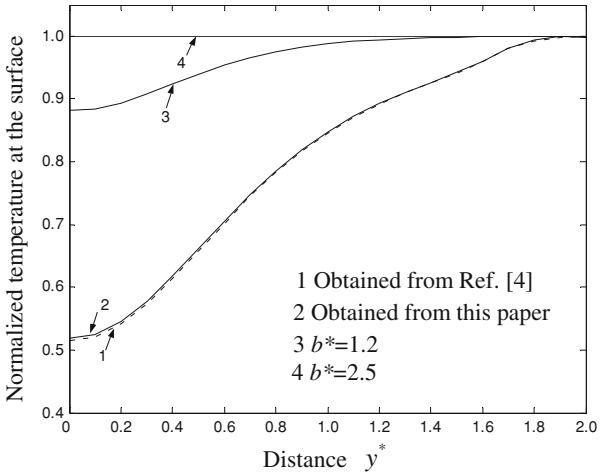

Fig. 3 Temperature at the semi-infinite surface of FGMs ($f = 1$ Hz, $k = 0$, $\sigma^* = 0$, $\lambda^* = D^* = 5.0$)

the temperature variation inside the materials. By making use of the variation of the temperature amplitude and the phase difference resulting from the defect, the imaging of thermal waves can be obtained. By measuring the temperature and phase variation at the surface of materials, the defect embedded beneath the surface can be estimated and evaluated.

To validate the present thermodynamic model, comparison with the previous literature is given. Figure 3 illustrates the temperature distribution at the surface of materials ($x = -b$) with parameters: $f = 1$ Hz, $k = 0$, $\sigma^* = 0$, $\lambda^* = 5.0$, $D^* = 5.0$, and $b^* = 1.0615$, which corresponds to the case of pure heat diffusion and the case without wave motion terms in the equation of heat conduction in homogeneous materials. In this case, the thermal conductivity and thermal diffusivity are given by $\lambda_0 = 0.4\,\mathrm{W \cdot m^{-1} \cdot K^{-1}}$ and $D_0 = 0.1\,\mathrm{m^2 \cdot s^{-1}}$, respectively. The radius of the cylindrical inclusion is $a = 0.65$ mm, and the embedded depth is $b = 0.69$ mm. It should be noted that $k = 0$ denotes the relaxation time of FGMs and inclusion is sufficiently small. These parameters are consistent with those in Ref. [1]. From Fig. 3, it can be seen that the computing results of the temperature at the surface of materials show good agreement with those in Ref. [4]. At the location of $(-b, 0)$, the temperature reaches the minimum. In Fig. 3, $b^* = 2.5$ means that the effect of the inclusion on the temperature disappears. As expected, the temperature at the surface has no variation. It is also clear that with the increase of the value of b, the variation of the temperature at the surface decreases. So, the effect of the inclusion on the temperature at the surface decreases with the increase of the distance between the inclusion and the semi-infinite surface.

Figure 4 illustrates the temperature distribution at the surface of FGMs with parameters: $\sigma^* = 0$, $b^* = 1.0615$, $k = 0$, and $f = 1$ Hz. As can be seen, the temperature above the conducting cylindrical inclusion decreases because of the existence of the inclusion. The greater the ratios of $\lambda^*$and D^*, the more evident the decrease of temperature at the surface. The physical explanation of this result is that, in the case of

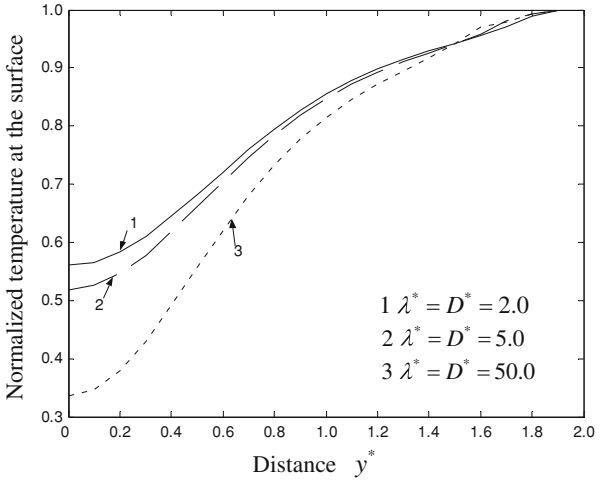

Fig. 4 Temperature at the semi-infinite surface of FGMs ($f = 1$ Hz, $k = 0, \sigma^* = 0, b^* = 1.0615$)

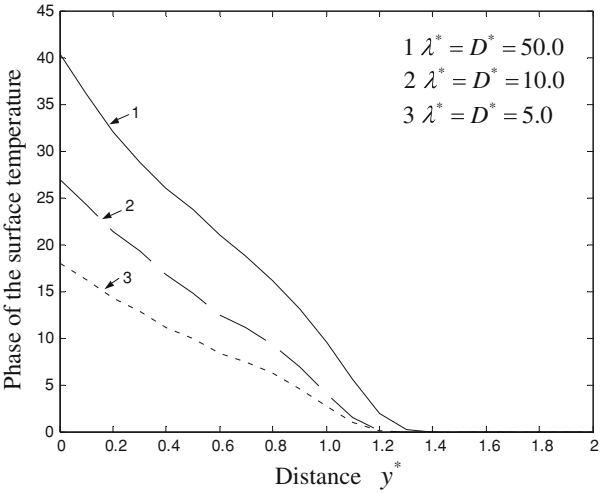

Fig. 5 Phase of temperature at the semi-infinite surface of FGMs ($f = 1$ Hz, $k = 0, \sigma^* = 0, b^* = 1.0615$)

a highly conducting cylinder, the incident and the scattered thermal waves are out of phase, so the superposition can be understood as a destructive interference. This is characteristic of curved buried features (cylinders, spheres, etc.), and it does not appear in planar features.

Figure 5 illustrates the phase change at the surface of FGMs with parameters: $\sigma^* = 0$, $b^* = 1.0615$, $k = 0$, and $f = 1$ Hz. As can be seen, the phase of temperature above the conducting cylindrical inclusion increases because of the existence of the inclusion. The greater the ratios of $\lambda^*$and D^*, the more evident the increase of the phase at the surface. Comparing with the results in Fig. 4, it is clear that the variations of material properties have greater influence on the phase of the surface temperature.

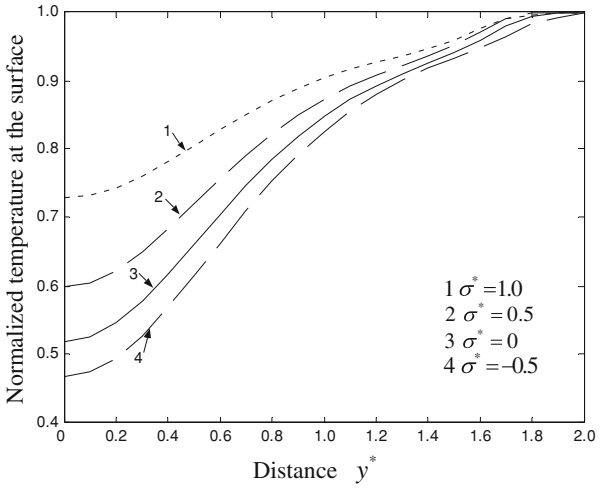

Fig. 6 Temperature at the semi-infinite surface of FGMs ($f = 1\,\text{Hz}, k = 0, \lambda^* = D^* = 5.0, b^* = 1.0615$)

The temperature distribution at the surface of FGMs with parameters: $b^* = 1.0615$, $k = 0$, $\lambda^* = 5.0$, $D^* = 5.0$, and $f = 1$ Hz is depicted in Fig. 6. It can be seen that the variation of the temperature above the conducting cylindrical inclusion increases with the decrease of the non-homogeneous parameter. With the increase of the value of y^*, the temperature at the surface becomes stable. When the non-homogeneous parameter is large, the variation of the thermal conductivity near the semi-infinite surface of FGMs is small. So, the effect of the conductive inclusion on the temperature at the surface is small. Thus, the decrease of the temperature above the conducting cylindrical inclusion is small.

The phase change at the surface of FGMs with parameters: $b^* = 1.0615$, $k = 0$, $\lambda^* = D^* = 5.0$, and $f = 1$ Hz is depicted in Fig. 7. It can be seen that the phase change of the temperature above the conducting cylindrical inclusion increases with the decrease of the non-homogeneous parameter. With the increase of the value of y^*, the phase change of the temperature at the surface becomes stable. Comparing with the results in Fig. 6, it is clear that the variation of the non-homogeneous parameter has greater influence on the phase of the surface temperature.

Figure 8 illustrates the temperature distribution at the surface of FGMs with parameters: $\sigma^* = 0$, $b^* = 1.0615$, $\lambda^* = D^* = 5.0$, and $k = 0$. It can be seen that the temperature above the conducting cylindrical inclusion decreases because of the existence of the inclusion. When the frequency of thermal waves is small, the decrease of the temperature above the conducting cylindrical inclusion is large. When the frequency of thermal waves is large, the decrease of the temperature above the conducting cylindrical inclusion is small. However, in the region of low frequency, the variation of the temperature at the surface with the value of y^* is small; in the region of high frequency, the variation of the temperature at the surface with the value of y^* is large.

Figure 9 shows the temperature distribution at the surface of FGMs with parameters: $b^* = 1.0615$, $k = 0$, $\lambda^* = 5.0$, $D^* = 5.0$, and $f = 5$ Hz. Comparing with the

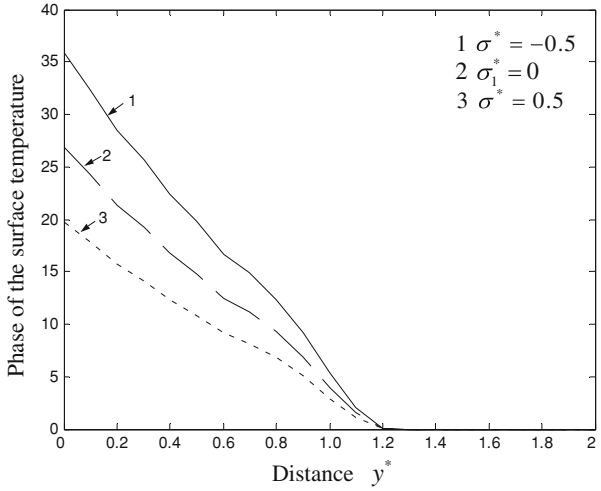

Fig. 7 Phase of temperature at the semi-infinite surface of FGMs ($f = 1\,\text{Hz}, k = 0, \lambda^* = D^* = 5.0, \sigma^* = 0, b^* = 1.0615$)

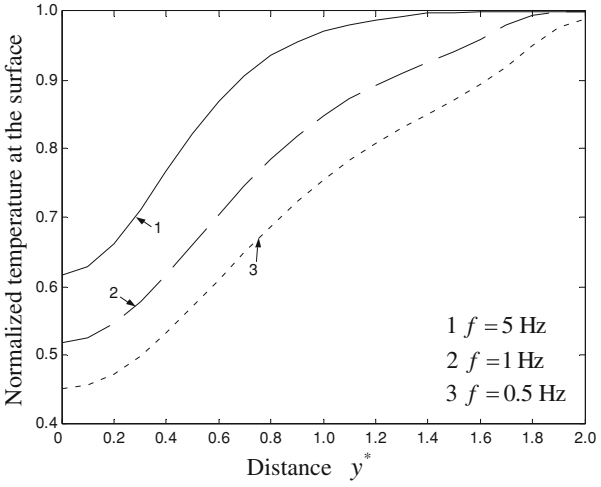

Fig. 8 Temperature at the semi-infinite surface of FGMs ($k = 0, \lambda^* = D^* = 5.0, \sigma^* = 0, b^* = 1.0615$)

results in Fig. 5, it can be seen that the effect of the non-homogeneous parameter on the temperature above the conducting cylindrical inclusion decreases with the increase of the incident frequency of thermal waves.

To find the effect of the relaxation time of the cylindrical inclusion on the temperature at the semi-infinite surface, Fig. 10 is given. It can be seen that with the increase of the relaxation time of the cylindrical inclusion, the temperature above the conducting cylindrical inclusion decreases greatly. So, the effect of the relaxation time of the cylindrical inclusion on the temperature increases with the value of τ^*. When the value

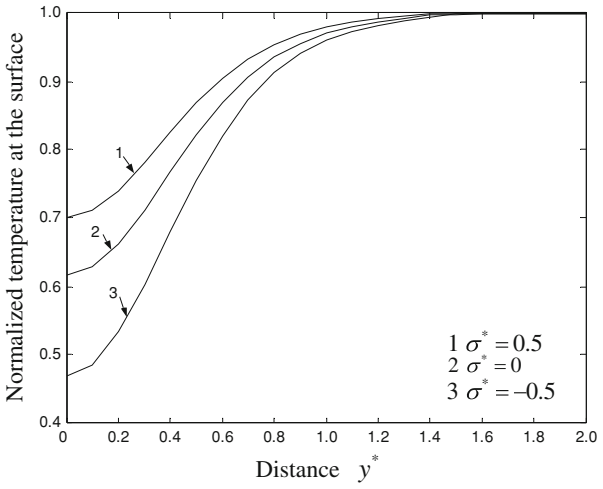

Fig. 9 Temperature at the semi-infinite surface of FGMs ($f = 5\,\text{Hz}, k = 0, \lambda^* = D^* = 5.0, b^* = 1.0615$)

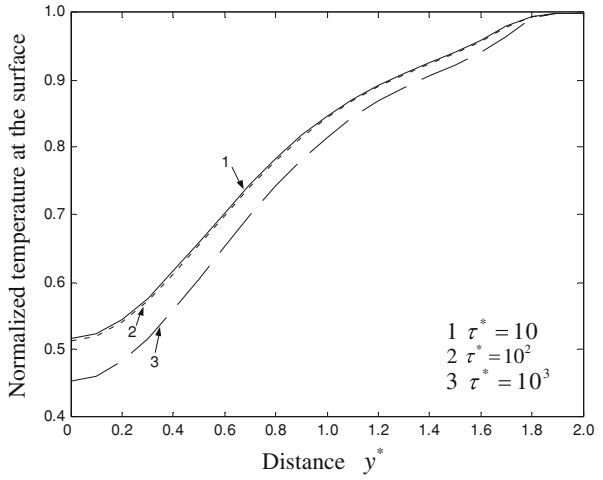

Fig. 10 Temperature at the semi-infinite surface of FGMs ($f = 1\,\text{Hz}, \lambda^* = D^* = 5.0, \sigma^* = 0, b^* = 1.0615$)

of τ^* is small, the variation of the relaxation time of the cylindrical inclusion has little effect on the temperature at the semi-infinite surface.

To find the effect of the relaxation time of the cylindrical inclusion on the temperature at the semi-infinite surface in the region of high frequency, Fig. 11 is given. Comparing with the results in Fig. 8, it is clear that the effect of the relaxation time of the cylindrical inclusion on the temperature above the conducting cylindrical inclusion increases with the increase of the wave frequency.

Finally, the effect of the relaxation time of the cylindrical inclusion on the phase change at the surface of FGMs is shown in Fig. 12. With the increase of the relaxation

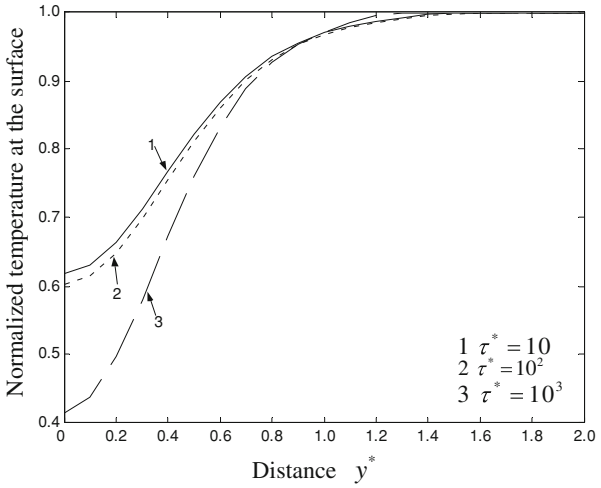

Fig. 11 Temperature at the semi-infinite surface of FGMs ($f = 5\,\text{Hz}, \lambda^* = D^* = 5.0, \sigma^* = 0, b^* = 1.0615$)

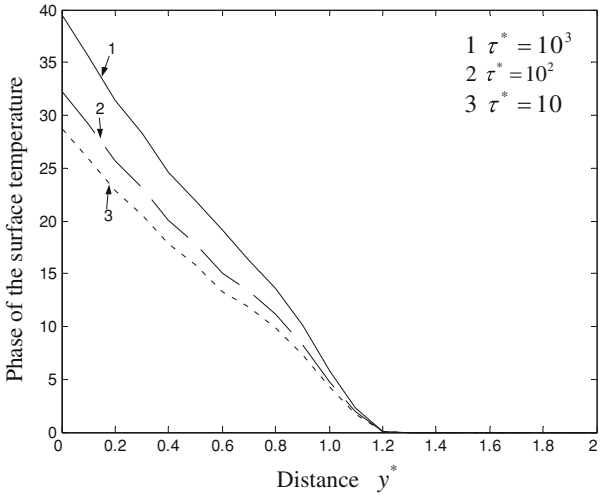

Fig. 12 Phase of temperature at the semi-infinite surface of FGMs ($f = 1\,\text{Hz}, \lambda^* = D^* = 5.0, \sigma^* = 0, b^* = 1.0615$)

time of the cylindrical inclusion, the effect of it on the phase change of the temperature at the surface increases. Comparing with the results in Fig. 10, it can be seen that the variation of the relaxation time of the cylindrical inclusion has greater influence on the phase of the surface temperature.

7 Conclusion

Applying the non-Fourier law of heat conduction, the propagation of thermal waves in semi-infinite FGMs with an embedded cylindrical inclusion has been considered, a general solution for the total temperature field in FGMs is presented. When the propagating speed of thermal waves is $c \to \infty$ and the non-homogeneous parameter is $\sigma \to 0$, the non-Fourier wave model of heat conduction in FGMs is reduced to the classical model of Fourier's thermal diffusion. The good agreement of the surface temperature of homogeneous materials with the previous literature confirms the validity of the present thermodynamic model.

It has been found that the effect of the inclusion on the temperature at the surface decreases with the increase of the distance between the inclusion and the semi-infinite surface. The temperature above the conducting cylindrical inclusion decreases because of the existence of the inclusion. The variation of temperature at the surface increases with increases in the ratios of λ^* and D^*. The temperature above the conducting cylindrical inclusion increases with the increase of the non-homogeneous parameter. The decrease of the temperature above the conducting cylindrical inclusion becomes small with the increase of the frequency of thermal waves is large, and the decrease of the temperature above the conducting cylindrical inclusion is small. The effect of the non-homogeneous parameter on the temperature above the conducting cylindrical inclusion also decreases with the increase of the incident frequency of thermal waves. The temperature above the conducting cylindrical inclusion decreases with the increase of the relaxation time of the cylindrical inclusion. With the increase of the wave frequency, the effect of the relaxation time of the cylindrical inclusion on the temperature increases. The material properties, the non-homogeneous parameter, and the frequency of thermal waves have similar effects on the phase of the surface temperature of FGMs. However, the phase change of the temperature is more sensitive to these parameters.

The results of this study can provide a theoretical foundation and references for the detection of defects by using laser heating in FGMs, and the analysis and computation of infrared thermal imaging in FGMs.

Acknowledgments The work is supported by the Natural Science Foundation for outstanding young researcher of Hebei Province China (Foundation No. A2009001624).

References

1. A. Ocariz, A. Sanchez-Lavega, A. Salazar, J. Appl. Phys. **81**, 7552 (1997)
2. A. Ocariz, A. Sanchez-Lavega, A. Salazar, J. Appl. Phys. **81**, 7561 (1997)
3. A. Salazar, A. Sanchez-Lavega, R. Celorrio, J. Appl. Phys. **93**, 4536 (2003)
4. J. M. Terrón, A. Sánchez-Lavega, A, Salazar, J. Appl. Phys. **89,** 5659 (2001)
5. J. M. Terrón, A. Sánchez-Lavega, A. Salazar, J. Appl. Phys. **87**, 2600 (2000)
6. A. Salazar, R. Celorrio, J. Appl. Phys. **100**, 113535 (2006)
7. A. Salazar, F. Garrido, R. Celorrio, J. Appl. Phys. **99**, 066116 (2006)
8. N. Madariaga, A. Salazar, J. Appl. Phys. **101**, 103534 (2007)
9. C. Wang, A. Mandelis, Y. Liu, J. Appl. Phys. **96**, 3756 (2004)
10. C. Wang, A. Mandelis, Y. Liu, J. Appl. Phys. **97**, 014911 (2005)
11. C. Wang, Y. Liu, A. Mandelis, J. Shen, J. Appl. Phys. **101**, 083503 (2007)

12. L.J. Gray, T. Kaplan, J.D. Richardson, ASME J. Appl. Mech. **70,** 543 (2003)
13. A. Salazar, A. Sanchez-Lavega, J. Appl. Phys. **93**, 4536 (2003)
14. T.Q. Qiu, C.L. Tien, Int. J. Heat Mass Transf. **35**, 719 (1992)
15. C. Korner, H.W. Bergmann, J. Appl. Phys. **67**, 397 (1998)
16. D.Y. Tzou, ASME J. Heat Transf. **117**, 8 (1995)
17. C. Cattaneo, Compte. Rend. **247**, 431 (1958)
18. X. Ma, H. Tan, J. Funct. Mater. **9**, 1507 (2006) (in Chinese)
19. B. Abdel-Hamid, Appl. Math. Model. **23**, 899 (1999)
20. V. Parameswaran, A. Shukla, ASME J. Appl. Mech. **69**, 240 (2002)
21. A. O. Ayhan, Int. J. Solids Struct. **44**, 8579 (2007)
22. F. Erdogan, Compos. Eng. **7**, 753 (1995)
23. M.A. Abramowitz, I.A. Stegun, *Handbook of Mathematical Functions* (Natl. Bur. Stand., Washington, DC, 1964)